Letter

Collector Droplet Behavior during Formation of Nanowire Junctions

Yanming Wang, Tomáš Šikola, and Miroslav Kolíbal*

Cite This: *J. Phys. Chem. Lett.* 2020, 11, 6498–6504

Read Online

ACCESS | Metrics & More | Article Recommendations | Supporting Information

ABSTRACT: Formation of nanowire networks is an appealing strategy for demonstrating novel phenomena at the nanoscale, e.g., detection of Majorana Fermions, as well as an essential step in realizing complex nanowire-based architectures. However, a detailed description of mechanisms taking place during growth of such complex structures is lacking. Here, the experimental observations of gold-catalyzed germanium nanowire junction formation are explained utilizing phase field modeling corroborated with real-time in situ scanning electron microscopy. When the two nanowires collide head on during the growth, we observe two scenarios. (i) Two catalytic droplets merge into one, and the growth continues as a single nanowire. (ii) The droplets merge and subsequently split again, giving rise to the growth of two daughter nanowires. Both the experiments and modeling indicate the critical importance of the liquid−solid growth interface anisotropy and the growth kinetics in facilitating the structural transition during the nanowire merging process.
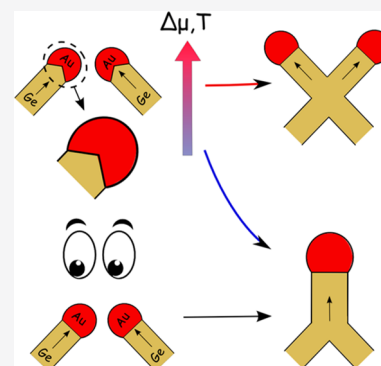
One of the envisioned unique advantages of one-dimensional nanostructures is their potential for three-dimensional stacking, which allows formation of complex architectures[1,2] for future electronics and nanophotonics. Crossed nanowire systems represent an effective platform for detection and manipulation of Majorana Fermions,[3−6] which have been intensively investigated for quantum computing considering their robust topological characteristics.[7,8] Also, for designing thermoelectric nanoscale systems, phonon transport engineering in one-dimensional systems provides a promising route,[9,10] where recent interest has been naturally drawn to nanowire junctions, going beyond a single wire architecture.[11−13] However, realizing precisely engineered networks of nanowire junctions is still challenging.

Fabrication of nanowire-based devices requires a synthesis approach that results in nanowire growth at positions predefined by lithography. In this regard, two techniques have become prominent. In a catalyst-free approach (also denoted as selective area epitaxy),[14] the nanowires nucleate within openings in an oxide or nitride mask and elongate in one dimension due to an interplay between the surface energies of different facets. The second approach utilizes the vapor−liquid−solid (VLS) mechanism,[15] which allows size-selective nucleation of nanowires from supersaturated catalyst nanoparticles. The nanoparticle size determines the nanowire diameter, and given that the nanoparticles can be placed onto a growth substrate with nanometer-scale precision,[16−18] VLS growth can achieve control of the nanowire size and location with the accuracy comparable with the catalyst-free approach. In both growth approaches, a nanowire junction can be subsequently formed by the collision of two nanowires growing in crystallographically well-defined growth directions toward each other. The feasibility of this process has been

demonstrated by utilizing either planar[19−22] or patterned[23,24] substrates to create dense arrays of nanowire junctions and even interconnected nanowire heterostructures.[25]

Despite these achievements, the final junction geometry is difficult to control. In the catalyst-free approach, "X", "V", and "Y" junction shapes have been reported,[5,26−28] among which a frequent observation is the "X" shape as a consequence of misalignment of the colliding nanowires. In this case, the nanowire top facet remains partially accessible to the growth species, and thus, both nanowires proceed in their original growth direction despite junction formation. On the contrary, in VLS growth, more complex shapes could be formed,[24,27] which is closely related to the droplet dynamics upon the droplet collision event. In general, this collision can be categorized into two types: tip to side and tip to tip. In the tip-to-side nanowire collisions, it has been demonstrated that the droplet of the colliding nanowire either slides down after hitting the other wire sidewall[20,23] or bounces off (forming a "K"-shaped junction).[22] In tip-to-tip collisions, the droplets have been reported to merge into one during a collision event,[29] which inevitably results in the decrease in nanowire density. This could be prevented by subsequent droplet splitting and formation of "X" junctions. Nevertheless, the governing mechanisms of junction formation in tip-to-tip collisions remain unexplored. Here, we investigate the tip-to-

tip collisions of Au-catalyzed Ge nanowires employing both phase field simulations and real-time in situ electron microscopy observations. We identify the critical importance of the shape of the liquid−solid growth interface and the growth kinetics in determining the droplet behavior and the final junction geometry. Our findings should shed more light on the very complex junction formation mechanism and inspire new strategies for optimizing synthesis pathways of nanowire networks.

To study the effect of the growth conditions on junction formation, and to avoid any possible influence of substrate prepatterning, we have utilized epi-ready Ge(100) wafers that were processed via a standard protocol before nanowire growth. Namely, the wafers were cleaned in acetone, IPA, and water, followed by immersion into an HF-modified[16] Au colloid solution (nanoparticles that are 20 or 80 nm in diameter) to deposit catalyst particles. The samples were immediately loaded into either a high-vacuum growth chamber or a modified scanning electron microscope (SEM) equipped with a germanium evaporation cell. Both experimental layouts are described in detail elsewhere (see Experimental Methods and ref 30).

In our experiments, gold-catalyzed germanium nanowire growth is achieved under high-vacuum conditions by evaporation from a solid source. This deposition technique is known to result in nanowires growing in the ⟨110⟩ direction, which exhibit a hexagonal cross section with four {111}-oriented and two {100}-oriented sidewalls.[31,32] The growth interface is not planar but consists of two inclined {111} planes, forming an inverted V shape.[31] Because of the crystal symmetry, four equivalently possible out-of-plane ⟨110⟩ growth directions exist, which enhances the probability of nanowire collisions (Figure 1), thus providing a nice
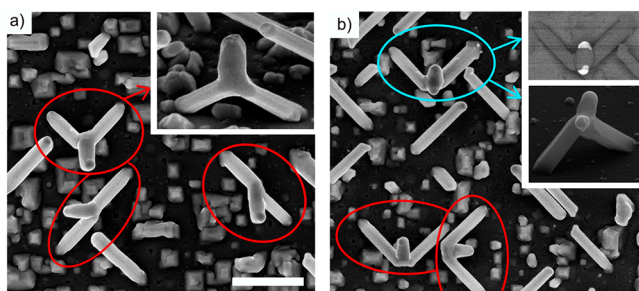

Figure 1. Nanowire junction formation at different growth rates. (a) At 380 °C, only merging is observed. (b) At 400 °C, in addition to merging splitting is also observed. The scale bar in the top view SEM images is 1 μm. The insets are inclined by 52°. The top inset in panel b is a Z-contrast image, showing the splitting of the catalyst. The bottom inset in panel b is a different nanowire than the one in the image.

playground for studying the junction formation phenomena. Figure 1a shows the growth conducted at 380 °C, slightly above the gold−germanium eutectic temperature. Under these conditions, "Y" junctions are formed (two nanowires merging into one). The nanowire originating from the collision point is larger in diameter (as the droplet volume increases after merging of the initial ones), and its growth direction is ⟨111⟩ with a rather complicated sidewall morphology.[30] If the growth is conducted at the higher temperature, "X" junctions are occasionally observed [the droplet splits into two after merging, and they catalyze the growth of two daughter

nanowires (see Figure 1b)]. Similar to the low-temperature collision event, the resulting nanowires grow into the ⟨111⟩ direction. The yield of "X" junctions on this sample is ∼15%, while on the sample prepared at a lower temperature, only "Y" junctions were found (slightly more than 100 nanowire junctions were inspected in each case). It should be noted that the geometrical configuration of the nanowires before junction formation does not have a decisive effect on the particular growth direction after junction formation; we observe all of the possible ⟨111⟩ directions (see Figure S1). For further discussion, it is also important to note that the higher growth temperature results in the higher growth rate of nanowires (see Figure S2 for growth rate quantification).[31] That is a direct consequence of the growth mechanism, because the growth rate is limited by the surface diffusion of germanium adatoms toward the catalytic droplet. The experiments also revealed that junction formation is not sensitive to the droplet diameter (within the studied range, 70−350 nm).

To unravel the effects of growth kinetics and the liquid−solid interface, we performed a series of phase field simulations[33,34] of nanowire collisions. We started with a single nanowire growth simulation, which imitated the Au-catalyzed ⟨110⟩-oriented Ge nanowire growth experiment using evaporation of Ge as the feed material. The simulated nanowire with a diameter of ∼120 nm continuously grew along the ⟨110⟩ orientation, reproducing well the morphology of the experimentally grown nanowires (e.g., showing six sidewall facets and an inverse V-shaped growth interface consisting of two {111} planes). We then placed these wires in various ways to construct the initial configurations for the subsequent collision simulations. As shown in Figure 2, the phase field model captures the nanowire junction formation process, predicting behavior similar to that of the experimental results. At low growth rates ($v \approx 5.3$ nm/min, estimated from Figure S2), the droplets merge into a single larger one, and the "Y" junction is formed as a result of continuing growth. If the growth rate is increased [$v \approx 8.7$ nm/min (Figure S2)], the droplet splits after merging, yielding the "X" junction formation if left developing further (Figure 2b). It should be noted that under a given condition, there is no variation in the type ("X" or "Y") of the junction structures that evolved in simulations (e.g., in the high-growth rate case, the model consistently predicts an "X" shape). That is in contrast to experiments, in which the yield of "X" junctions is much smaller. This discrepancy comes from the deterministic nature of our current model, where the local environmental and thermal fluctuations in experimental growth systems are not specifically considered.

The simulation results, together with experimental observations, support the hypothesis that the droplet splitting is an activated process, requiring additional energy to overcome the related kinetic barrier. This is achieved by increasing the growth temperature in the experiment or by directly increasing the chemical potential driving force in the simulation. These two quantities can be satisfactorily correlated by comparing their effects on the nanowire growth rate (Figure S2). Such an approach provides a link between experiments and simulations, overcoming the difficulty in directly quantifying the chemical potential driving force from an experiment.

The simulation outcomes predict very unusual droplet wetting states immediately after the collision of nanowires. These droplet configurations (Figure 2) thus question a
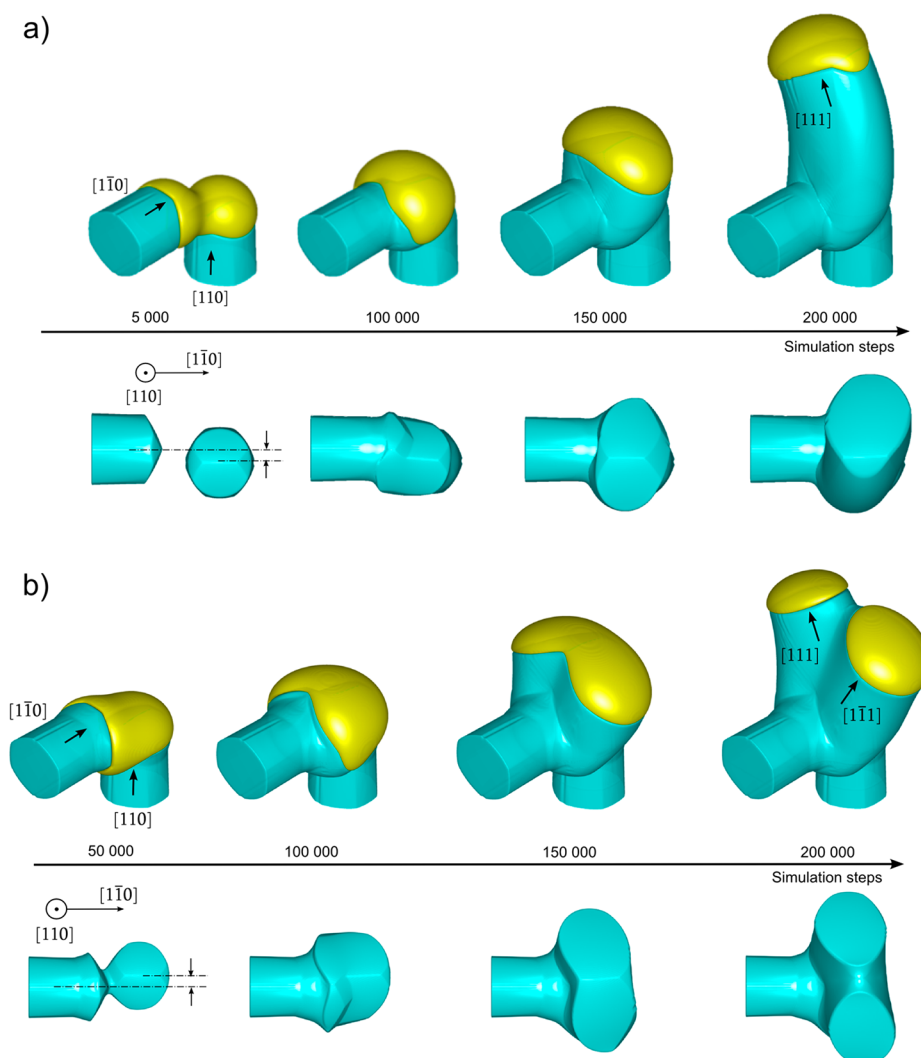
Figure 2. Phase field simulations of nanowire junction formation at different growth rates. The diameter of the nanowires is around 120 nm and is kept the same in all simulations throughout this paper. (a) At the slow growth rate (∼5.3 nm/min), the droplets catalyzing the growth of the initial ⟨110⟩-oriented nanowires are merged into one, the "Y" junction is formed, and the nanowire grows in the ⟨111⟩ direction. (b) At a higher growth rate (∼8.7 nm/min), the merged droplet is prone to splitting, resulting in the formation of the "X" junction as two nanowires grow after the collision event. The growth orientation of newly formed nanowires is changed to ⟨111⟩. In panels a and b, the top row shows tilted side views and bottom row top views, including the coordination system. In both cases, the colliding nanowires are slightly misaligned to reflect a common experimental off-axis nanowire arrangement.

common view of a nearly hemispherical droplet wetting of a nanowire tip during growth. To verify if these intermediate droplet states are plausible, we have conducted the growth in a scanning electron microscope to obtain a real-time view of the collision event. Utilizing the same evaporation cell and sample heating element, we were able to establish the same growth conditions as in the ex situ growth chamber. The image sequences taken under the experimental growth conditions relevant to Figure 1a ("Y" junction formation) and Figure 1b ("X" junction formation) are shown in panels a–c of Figure 3. The droplet wetting configurations captured after the collision event exhibit striking similarities with those calculated by the phase field model. Both the real-time imaging and modeling suggest that the complex wetting shapes are probably possible due to strong pinning of the liquid catalyst to the edges of the original growth interface(s).

Here we further discuss the growth direction change after the collision event. The splitting of the droplet naturally results in the formation of two new liquid−solid growth interfaces

with a ⟨111⟩ orientation. The two wires growing after the splitting thus grow in the ⟨111⟩ direction, in contrast to the initial ⟨110⟩ orientation. It should be noted that the ⟨111⟩-oriented nanowires exhibit a morphology different from that of the ⟨110⟩ direction, but just as the case of the ⟨110⟩-oriented wires, the simulation-predicted morphology[34] reasonably matches that observed experimentally.[30] Extensive modeling has shown that kinking from ⟨110⟩ to ⟨111⟩ is feasible under the most experimental conditions. There is, however, one exception. Figures S3 and S4 show the case of perfectly aligned colliding nanowires, again under the conditions of slow and fast growth. The resulting junction shape is not affected by the geometry of the collision (i.e., the angle between the colliding nanowires); however, in the case of slow growth, the kinking of the resulting nanowire toward ⟨111⟩ does not take place. Despite other effects, e.g., nanowire diameter,[33] these additional simulations we have performed suggest that kinking after the collision event may be related to the misalignment of the colliding nanowires. As a consequence of the off-axis collision,
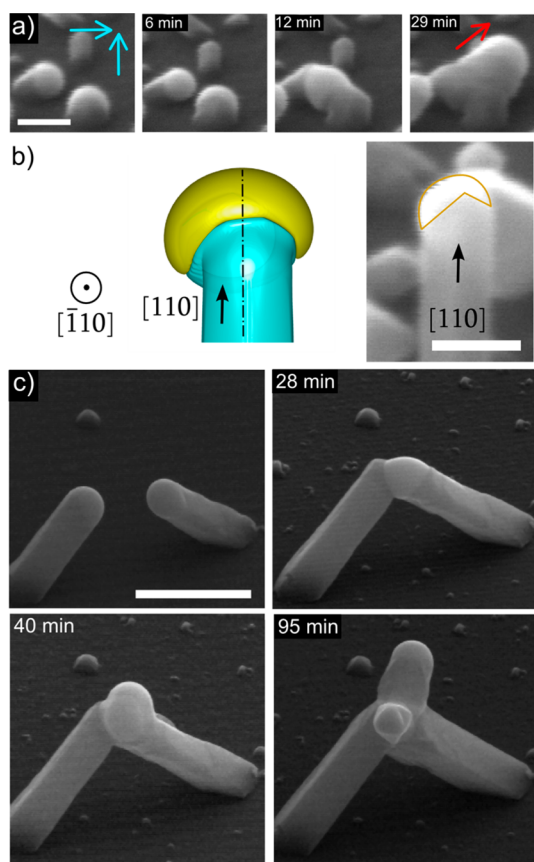
Figure 3. Real-time observation of droplet behavior during a head-on collision event. (a) The image sequence was taken under growth conditions similar to those presented in Figure 1a. The scale bar is 100 nm. (b) Different view of the nanowire collision from Figure 2a, showing the liquid−solid growth interface with an asymmetric shape (100000 simulation steps in panel a), which forces the droplet to pin in an off-balance position. This simulation snapshot is corroborated by the real-time microscopy image, which reveals the off-balance position of the initially symmetric droplet just after a collision with a larger nanowire from behind (the SEM image is tilted by 52°, and the scale bar is 100 nm). The interface asymmetry leads to the diminishing of one of the {111} facets (in agreement with experimental observations[31] and theoretical modeling[35]). (c) At a higher temperature (420 °C), droplet splitting occurs. The scale bar is 1 μm. In panels a and c, the merged droplet exhibits an elongated shape pinned to both growth interfaces, strikingly similar to the phase field modeling results.

the droplet wetting configuration changes to an asymmetric one, which results in the subsequent growth direction change (Figures 2a and 3b). A similar kinking phenomenon is captured by applying external force perturbation on the droplet to mimic the droplet oscillation (see Figure S5 and ref 35). Additionally, such behavior indicates that the ⟨110⟩ direction could be a metastable growth direction, while the ⟨111⟩ direction represents a stable state.

Finally, additional simulations reveal that for the occurrence of the splitting process, the droplet−nanowire contact geometry is one critical factor in lowering the related kinetic barrier. This finding is verified by our simulations of the evolution of a droplet wetting of two crossed nanowires with flat liquid−solid interfaces [by assigning isotropic interfacial energies in the model (Figure 4)]. In this case, despite the higher chemical potential driving force that is anticipated to
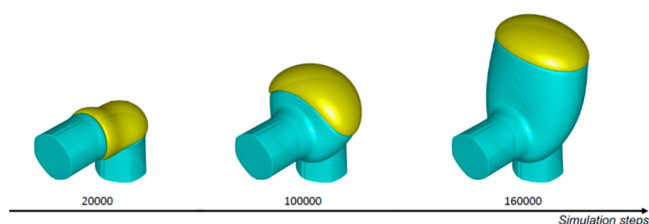

Figure 4. Phase field simulation of nanowire junction evolution if the anisotropy of interfacial energies is switched off (hence, isotropic interfacial energies result in a flat growth interface). The splitting does not occur despite the larger growth rate (compare to Figure 2b, where the growth rate is the same).

promote splitting (Figure 2b), the droplet does not split, and the nanowire junction evolves toward a "Y" shape. This result emphasizes the importance of growth interface anisotropy as a key influential factor in determining the final nanowire junction shape. Presumably, the inverse-V-shaped liquid−solid interface can facilitate the formation of "X" junctions, by offering a kinetic pathway for droplet splitting with a lower activation energy.

The tendency of the droplet to split could also be dependent on other factors that are not inspected here. For example, the surface free energy of the liquid can affect the droplet stability on top of a nanowire. It has been theoretically proposed that the splitting of the droplet may be energetically favorable if catalysts with a low surface energy are used for promoting nanowire growth,[36,37] though such behavior was observed very rarely.[37] The effect of the surface energy of the liquid on droplet stability is size-dependent, which is found to be more profound for very small nanowire diameters. In our experiments, we have not observed noticeable size effects (our nanowires have diameters of 70−350 nm), but this may not be the case for much smaller droplet diameters. However, studying the size effects on splitting is beyond the scope of this paper.

The conclusions derived from our simulations can possibly be extended to other material systems, e.g., III−V nanowires that predominantly grow in ⟨111⟩ growth directions with the liquid−solid interface formed by a {111} plane. Depending on the growth conditions, this growth plane may become truncated; the droplet supersaturation determines the extension of this truncation.[35] The truncation facets have been observed experimentally, e.g., for GaAs,[38] GaP,[39] InAs,[40] and sapphire,[41] and similarly in computer simulations.[35,42] On the basis of our predictive results, one could expect that possibly the "X" junctions (resulting from the splitting of a merged droplet) can also be seen in other VLS-grown nanowires with sufficiently large growth plane truncation (i.e., anisotropic liquid−solid interface) under specific growth conditions. In fact, the junction shapes in some of the systems have been reported very recently.[24]

In summary, we have shown that the nanowires grown by the vapor−liquid−solid approach can be engineered to form junctions of a desirable shape by carefully tuning the experimental conditions. The experimental results are corroborated by extensive phase field simulations, which have unravelled the crucial importance of the growth interface anisotropy and the growth kinetics with respect to the resulting junction shape. The droplets on top of merged wires are more prone to splitting if the liquid−solid interface evolves toward an anisotropic shape, which is inherent to some catalyst/

nanowire systems (in the case of Au-catalyzed Ge nanowires, as shown here, the growth interface is V-shaped along the $\langle 110 \rangle$ orientation) or can be experimentally controlled by altering the growth conditions (in the case of III−V nanowires, large droplet supersaturation results in significant truncation of the top nanowire facet beneath the droplet). Our findings are thus not limited within the material system studied in this paper but should be more generally applicable to other nanowire systems, as useful guidelines for designing and tailoring junction geometries.

■ EXPERIMENTAL METHODS

Phase Field Simulations. A three-dimensional multiphase field model,[34,43] implemented in the MD++ framework (http://micro.stanford.edu/MDpp),[44] was adopted to study the formation of nanowire junctions during VLS growth. Choosing the phase field $\phi_i(\mathbf{x})$ (i = L, S, or V for the liquid, solid, or vapor phase, respectively) as the fundamental degrees of the freedom, we can describe the total free energy of the system in functional form in eq 1[34]

$$
\begin{aligned}
F[\phi_L(\mathbf{x}), \phi_S(\mathbf{x}), \phi_V(\mathbf{x})] &= F_{\text{interfacial}} + F_{\text{chemical}} + F_{\text{force}} \\
&+ F_{\text{penalty}} = \sum_{i=L,S,V} \int U_i \phi_i^2 (1 - \phi_i)^2 + \epsilon_i^2(\mathbf{n}) |\nabla \phi_i|^2 \, d^3\mathbf{x} \\
&+ \sum_{i=L,S,V} \int \mu_i C(\phi_i) \, d^3\mathbf{x} + \int \vec{\alpha} \cdot (\mathbf{x} - \mathbf{x_0}) C(\phi_L) \, d^3\mathbf{x} \\
&+ \int P \phi_L^2 \phi_S^2 \phi_V^2 \, d^3\mathbf{x}
\end{aligned}
\tag{1}
$$

which includes the contributions from interfacial energies, chemical potentials, external forces on the droplet, and a penalty term for preventing unphysical phase mixing behaviors. The key model parameters, as explained in the Supporting Information and listed in Table S1, were taken from ref 34 to reproduce the anisotropic interfacial energies of the Au−Ge system (U_i and ϵ_{i0}^2 were scaled to keep the smoothness of the phase field profile at the interface). Setting the chemical potential of the solid phase to 0 as the reference, a constant chemical potential density of the vapor phase μ_V was set to 0.0104 and 0.0168 eV/nm^3 to provide the driving force for nanowire slow and fast growth, respectively. The dimensions of the simulation cell were set to 550 nm (x) × 650 nm (y) × 550 nm (z), with directions of the x, y, and z axes corresponding to [001], [110], and [1$\bar{1}$0] nanowire crystallographic orientations, respectively. Keeping the liquid droplet volume constant (via adjusting the liquid chemical potential μ_L using the method of Lagrange multipliers), a series of phase field simulations were performed with a time step of 0.02 s, to match the experimental time scale (Figure S2). At each time step, the variational derivatives of F with respect to ϕ_i were calculated to govern the system evolution to the lower-free energy direction. An Euler forward time integrator was then employed to update the values of ϕ_i accordingly. The simulation snapshots were recorded and plotted using *Matlab*, in the form of isosurfaces at a ϕ_i of 0.5 (an order parameter denoting the phase of materials), where i = L or S (liquid or solid, respectively).

Nanowire Growth. Nanowire growth was performed in a UHV chamber and in a modified SEM chamber. The heating stage (pyrolytic boron nitride-based heating element) and germanium evaporator (in-house built) were the same in both chambers to ensure the reproducibility of the results. The

sample temperature was calibrated before the experiment in both systems by a thermocouple and independently verified by a pyrometer. The resulting calibration curve (temperature/current passing the heating element) was validated in a separate SEM experiment using temperature-indicating suspensions. The evaporation rate was controlled by changing the evaporator crucible temperature and calibrated before the experiment using a crystal quartz thickness monitor. The incidence angle of germanium atoms on the sample with respect to the sample normal was 70°. In the case of real-time SEM experiments, the evaporation geometry was the same, and the electron beam was incident under 52° to the sample normal.

■ ASSOCIATED CONTENT

Ⓢ Supporting Information

The Supporting Information is available free of charge at https://pubs.acs.org/doi/10.1021/acs.jpclett.0c01653.

> Additional experimental and modeling results in different nanowire geometric configurations, growth rate evaluation, and parameters of the phase field model (PDF)

■ AUTHOR INFORMATION

Corresponding Author

Miroslav Kolíbal − *Institute of Physical Engineering and CEITEC BUT, Brno University of Technology, 616 69 Brno, Czech Republic;* ⊙ orcid.org/0000-0002-2751-5608; Email: kolibal.m@fme.vutbr.cz

Authors

Yanming Wang − *Department of Materials Science and Engineering, Massachusetts Institute of Technology, Cambridge, Massachusetts 02139, United States;* ⊙ orcid.org/0000-0002-0912-681X

Tomáš Šikola − *Institute of Physical Engineering and CEITEC BUT, Brno University of Technology, 616 69 Brno, Czech Republic*

Complete contact information is available at:
https://pubs.acs.org/10.1021/acs.jpclett.0c01653

Notes

The authors declare no competing financial interest.

■ REFERENCES

(1) Zhou, J.; Ding, Y.; Deng, S. Z.; Gong, L.; Xu, N. S.; Wang, Z. L. Three-dimensional Tungsten Oxide Nanowire Networks. *Adv. Mater.* **2005**, *17*, 2107−2110.

(2) Gedamu, D.; Paulowicz, I.; Kaps, S.; Lupan, O.; Wille, S.; Haidarschin, G.; Mishra, Y. K.; Adelung, R. Rapid fabrication technique for interpenetrated ZnO nanotetrapod networks for fast UV sensors. *Adv. Mater.* **2014**, *26*, 1541−1550.

(3) Deng, M. T.; Vaitiekėnas, S.; Hansen, E. B.; Danon, J.; Leijnse, M.; Flensberg, K.; Nygård, J.; Krogstrup, P.; Marcus, C. M. Majorana bound state in a coupled quantum-dot hybrid-nanowire system. *Science* **2016**, *354*, 1557−1562.

(4) Fadaly, W. M. T.; Zhang, H.; Conesa-Boj, S.; Car, D.; Gül, O.; Plissard, S. R.; Op het Veld, R. L. M.; Kölling, S.; Kouwenhoven, L. P.; Bakkers, E. P. A. M. Observation of Conductance Quantization in InSb Nanowire Networks. *Nano Lett.* **2017**, *17*, 6511−6515.

(5) Gazibegovic, S.; et al. Epitaxy of advanced nanowire quantum devices. *Nature* **2017**, *548*, 434−438.

(6) Zhang, H.; Liu, D. E.; Wimmer, M.; Kouwenhoven, L. Next steps of quantum transport in Majorana nanowire devices. *Nat. Commun.* **2019**, *10*, 5128.

(7) Gül, O.; Zhang, H.; Bommer, J. D. S.; de Moor, M. W. A.; Car, D.; Plissard, S. R.; Bakkers, E. P. A. M.; Geresdi, A.; Watanabe, K.; Taniguchi, T.; Kouwenhoven, L. P. *Nat. Nanotechnol.* **2018**, *13*, 192.

(8) Car, D.; Conesa-Boj, S.; Zhang, H.; Op het Veld, R. L. M.; de Moor, M. W.A.; Fadaly, E. M.; Gül, O.; Kölling, S.; Plissard, S. R.; Toresen, V.; Wimmer, M. T.; Watanabe, K.; Taniguchi, T.; Kouwenhoven, L. P.; Bakkers, E. P. A. M. InSb Nanowires with Built-In Ga$_x$In$_{1-x}$Sb Tunnel Barriers for Majorana Devices. *Nano Lett.* **2017**, *17*, 721−727.

(9) Boukai, A. I.; Bunimovich, Y.; Tahir-Kheli, J.; Yu, J.-K.; Goddard III, W. A.; Heath, J. R. *Nature* **2008**, *451*, 168−171.

(10) Hochbaum, A. I.; Chen, R.; Delgado, R. D.; Liang, W.; Garnett, E. C.; Najarian, M.; Majumdar, A.; Yang, P. *Nature* **2008**, *451*, 163−168.

(11) Ma, D.; Ding, H.; Meng, H.; Feng, L.; Wu, Y.; Shiomi, J.; Yang, N. Nano-cross-junction effect on phonon transport in silicon nanowire cages. *Phys. Rev. B: Condens. Matter Mater. Phys.* **2016**, *94*, 165434.

(12) Pennelli, G.; Totaro, M.; Piotto, M.; Bruschi, P. Seebeck coefficient of nanowires interconnected into large area networks. *Nano Lett.* **2013**, *13*, 2592−2597.

(13) Ma, D.; Arora, A.; Deng, S.; Xie, G.; Shiomi, J.; Yang, N. Quantifying phonon particle and wave transport in silicon nano-phononic metamaterial with cross junction. *Mater. Today Phys.* **2019**, *8*, 56−61.

(14) Motohisa, J.; Noborisaka, J.; Takeda, J.; Inari, M.; Fukui, T. Catalyst-free selective-area MOVPE of semiconductor nanowires on (111)B oriented substrates. *J. Cryst. Growth* **2004**, *272*, 180.

(15) Wagner, R. S.; Ellis, W. C. Vapor-Liquid-Solid Mechanism of Single Crystal Growth. *Appl. Phys. Lett.* **1964**, *4*, 89−90.

(16) Kolíbal, M.; Konečný, M.; Ligmajer, F.; Škoda, D.; Vystavěl, T.; Zlámal, J.; Varga, P.; Šikola, T. Guided Assembly of Gold Colloidal Nanoparticles on Silicon Substrates Prepatterned by Charged Particle Beams. *ACS Nano* **2012**, *6*, 10098−10106.

(17) Asbahi, M.; et al. Large Area Directed Self-Assembly of Sub-10 nm Particles with Single Particle Positioning Resolution. *Nano Lett.* **2015**, *15*, 6066−6070.

(18) Zhang, H.; Cadusch, J.; Kinnear, C.; James, T.; Roberts, A.; Mulvaney, P. Direct Assembly of Large Area Nanoparticle Arrays. *ACS Nano* **2018**, *12*, 7529−7537.

(19) Plissard, S.; et al. Formation and electronic properties of InSb nanocrosses. *Nat. Nanotechnol.* **2013**, *8*, 859−864.

(20) Kang, J.-H.; et al. Crystal Structure and Transport in Merged InAs Nanowires MBE Grown on (001) InAs. *Nano Lett.* **2013**, *13*, 5190−5196.

(21) Car, D.; Wang, J.; Verheijen, M. A.; Bakkers, E. P. A. M.; Plissard, S. Rationally designed single-crystalline nanowire networks. *Adv. Mater.* **2014**, *26*, 4875−4879.

(22) Kang, J.-H.; Galicka, M.; Kacman, P.; Shtrikman, H. Wurtzite/Zinc-Blende 'K'-shape InAs Nanowires with Embedded Two-Dimensional Wurtzite Plates. *Nano Lett.* **2017**, *17*, 531−537.

(23) Dalacu, D.; Kam, A.; Austing, D. G.; Poole, P. J. Droplet Dynamics in Controlled InAs Nanowire Interconnections. *Nano Lett.* **2013**, *13*, 2676−2681.

(24) Kang, J.-H.; Krizek, F.; Zaluska-Kotur, M.; Krogstrup, P.; Kacman, P.; Beidenkopf, H.; Shtrikman, H. Au-Assisted Substrate-Faceting for Inclined Nanowire Growth. *Nano Lett.* **2018**, *18*, 4115−4122.

(25) Rieger, T.; Rosenbach, D.; Mussler, G.; Schäpers, T.; Grützmacher, D.; Lepsa, M. I. Simultaneous Integration of Different Nanowires on Single Textured Si (100) Substrates. *Nano Lett.* **2015**, *15*, 1979−1986.

(26) Heedt, S.; Vakulov, D.; Rieger, T.; Rosenbach, D.; Trellenkamp, S.; Grützmacher, D.; Lepsa, M. I.; Schäpers, T. Electronic Properties of Complex Self-Assembled InAs Nanowire Networks. *Adv. Electron. Mater.* **2016**, *2*, 1500460.

(27) Rieger, T.; Rosenbach, D.; Vakulov, D.; Heedt, S.; Schäpers, T.; Grützmacher, D.; Lepsa, M. I. Crystal Phase Transformation in Self-Assembled InAs Nanowire Junctions on Patterned Si Substrates. *Nano Lett.* **2016**, *16*, 1933−1941.

(28) Krizek, F.; Kanne, T.; Razmadze, D.; Johnson, E.; Nygård, J.; Marcus, C. M.; Krogstrup, P. Growth of InAs Wurtzite Nanocrosses from Hexagonal and Cubic Basis. *Nano Lett.* **2017**, *17*, 6090−6096.

(29) Tang, J.; Maurice, J.-L.; Chen, W.; Misra, S.; Foldyna, M.; Johnson, E. V.; Roca i Cabarrocas, P. Plasma-Assisted Growth of Silicon Nanowires by Sn Catalyst: Step-by-step observation. *Nanoscale Res. Lett.* **2016**, *11*, 455.

(30) Kolíbal, M.; Pejchal, T.; Vystavěl, T.; Šikola, T. The Synergic Effect of Atomic Hydrogen Adsorption and Catalyst Spreading on Ge Nanowire Growth Orientation and Kinking. *Nano Lett.* **2016**, *16*, 4880−4886.

(31) Kolíbal, M.; Kalousek, R.; Vystavěl, T.; Novák, L.; Šikola, T. Controlled faceting in < 110> germanium nanowire growth by switching between vapor-liquid-solid and vapor-solid-solid growth. *Appl. Phys. Lett.* **2012**, *100*, 203102.

(32) Schmidtbauer, J.; Bansen, R.; Heimburger, R.; Teubner, T.; Boeck, T.; Fornari, R. Germanium nanowire growth controlled by surface diffusion effects. *Appl. Phys. Lett.* **2012**, *101*, No. 043105.

(33) Li, Y.; Wang, Y.; Ryu, S.; Marshall, A. F.; Cai, W.; McIntyre, P. C. Spontaneous, defect-free kinking via capillary instability during vapor−liquid−solid nanowire growth. *Nano Lett.* **2016**, *16*, 1713−1718.

(34) Wang, Y.; McIntyre, P. C.; Cai, W. Phase field model for morphological transition in nanowire vapor−liquid−solid growth. *Cryst. Growth Des.* **2017**, *17*, 2211−2217.

(35) Schwarz, K. W.; Tersoff, J. Elementary processes in nanowire growth. *Nano Lett.* **2011**, *11*, 316−320.

(36) Roper, S. M.; Anderson, A. M.; Davis, S. H.; Voorhees, P. W. Radius selection and droplet unpinning in vapor-liquid-solid-grown nanowires. *J. Appl. Phys.* **2010**, *107*, 114320.

(37) Nebol'sin, V. A.; Dunaev, A. I.; Dolgachev, A. A.; Zavalishin, M. A.; Sladkikh, G. A.; Korneeva, V. V.; Eframeev, A. Yu. Critical parameters of the vapor-liquid-solid growth of silicon whiskers. *Inorg. Mater.* **2011**, *47*, 11−15.

(38) Jacobsson, D.; Panciera, F.; Tersoff, J.; Reuter, M. C.; Lehmann, S.; Hofmann, S.; Dick, K. A.; Ross, F. M. Interface dynamics and crystal phase switching in GaAs nanowires. *Nature* **2016**, *531*, 317−322.

(39) Wen, C.-Y.; Tersoff, J.; Hillerich, K.; Reuter, M. C.; Park, J. H.; Kodambaka, S.; Stach, E. A.; Ross, F. M. Periodically changing morphology of the growth interface in Si, Ge and GaP nanowires. *Phys. Rev. Lett.* **2011**, *107*, No. 025503.

(40) Tornberg, M.; Dick, K. A.; Lehmann, S. Thermodynamic stability of gold-assisted InAs nanowire growth. *J. Phys. Chem. C* **2017**, *121*, 21678−21684.

(41) Oh, S. H.; Chisholm, M. F.; Kauffmann, Y.; Kaplan, W. D.; Luo, W.; Rühle, M.; Scheu, C. Oscillatory mass transport in vapor-

liquid-solid growth of sapphire nanowires. *Science* **2010**, *330*, 489−493.

(42) Haxhimali, T.; Buta, D.; Asta, M.; Voorhees, P. W.; Hoyt, J. J. Size-dependent nucleation kinetics at nonplanar nanowire growth interfaces. *Phys. Rev. E* **2009**, *80*, No. 050601(R).

(43) Wang, Y.; Ryu, S.; McIntyre, P. C.; Cai, W. A three-dimensional phase field model for nanowire growth by the vapor−liquid−solid mechanism. *Modell. Simul. Mater. Sci. Eng.* **2014**, *22*, No. 055005.

(44) Cai, W. *MD++ molecular dynamics simulations package* (accessed 2020-09-07).